Open access • Journal Article • DOI:10.1021/JP057435Z

Silica-coated CdTe quantum dots functionalized with thiols for bioconjugation to IgG proteins. — Source link

Abraham Wolcott, Daniele Gerion, Micah P. Visconte, Jia Sun ...+3 more authors

Institutions: University of California, Santa Cruz

Published on: 28 Feb 2006 - Journal of Physical Chemistry B (American Chemical Society)

Topics: Quantum dot

Silica-Coated CdTe Quantum Dots Functionalized with Thiols for Bioconjugation to IgG Proteins

Abraham Wolcott,[†] Daniele Gerion,[‡] Micah Visconte,[†] Jia Sun,[†] Adam Schwartzberg,[†] Shaowei Chen,[†] and Jin Z. Zhang*,[†]

Department of Chemistry and Biochemistry, University of California, Santa Cruz, Santa Cruz, California 95064, and Physics and Advanced Technology, Lawrence Livermore National Laboratory, Livermore, California 94550.

Received: December 21, 2005; In Final Form: January 26, 2006

Quantum dots (QDs) have been increasingly used in biolabeling recently as their advantages over molecular fluorophores have become clear. For bioapplications QDs must be water-soluble and buffer stable, making their synthesis challenging and time-consuming. A simple aqueous synthesis of silica-capped, highly fluorescent CdTe quantum dots has been developed. CdTe QDs are advantageous as the emission can be tuned to the near-infrared where tissue absorption is at a minimum, while the silica shell can prevent the leakage of toxic Cd^{2+} and provide a surface for easy conjugation to biomolecules such as proteins. The presence of a silica shell of 2−5 nm in thickness has been confirmed by transmission electron microscopy and atomic force microscopy measurements. Photoluminescence studies show that the silica shell results in greatly increased photostability in Tris−borate−ethylenediaminetetraacetate and phosphate-buffered saline buffers. To further improve their biocompatibility, the silica-capped QDs have been functionalized with poly(ethylene glycol) and thiol-terminated biolinkers. Through the use of these linkers, antibody proteins were successfully conjugated as confirmed by agarose gel electrophoresis. Streptavidin−maleimide and biotinylated polystyrene microbeads confirmed the bioactivity and conjugation specificity of the thiolated QDs. These functionalized, silica-capped QDs are ideal labels, easily synthesized, robust, safe, and readily conjugated to biomolecules while maintaining bioactivity. They are potentially useful for a number of applications in biolabeling and imaging.

1. Introduction

Semiconductor nanoparticles or quantum dots (QDs) have shown great promise for biolabeling of DNA, proteins, and cells.[1−4] They offer advantages including tunable emission spectra, high photostability, resistance to photobleaching, and controllable surface characteristics.[5−7] Semiconductor QDs are beholden to strong quantum confinement effects, and their emission spectra are size-dependent.[8] In comparison to organic fluorophores, semiconductor nanoparticles provide a competitive alternative for biomolecular imaging and analysis.[9] For instance, the ability to conduct bioimaging over extended periods of time without decomposition was demonstrated with phosphine-coated QDs for in vivo site-directed surgeries.[10]

The control over surface properties of QDs is especially crucial to maintain desirable fluorescent properties and aqueous solubility. Functionalization of the nanoparticle surface is also important to prepare the surface to be exploited for bioconjugation purposes. High quantum yields have been reported in the range of 10−50% depending upon the quality and surface properties of the QDs.[5−8] Semiconductor nanoparticles, especially the much lauded CdSe/ZnS core/shell system, are typically synthesized in organic solvents[8] and require an exchange of capping agents to allow for aqueous solubility. Ligand exchange can be time-consuming, difficult and can decrease the QD stability.

The ability to conjugate QDs to biomolecules was first performed by Bruchez[4] and Chan[2] in 1998 and has since been greatly exploited in a variety of fluoroimmunoassay, cell imaging, and DNA sequencing techniques. Different conjugation protocols have been engineered to specifically bind biomolecules to QDs.[11−13] Binding through electrostatic interactions using positively charged recombinant proteins and negatively charged dihydrolipoic acid (DHLA)-capped CdSe/ZnS QDs was employed to effectively perform toxin analysis of chlorera toxin, ricin, shiga-like toxin 1, and staphylococcal eneterotoxin B using QDs emitting at 510, 550, 590, and 610 nm for sandwich immunoassays.[11] Covalently bonded QDs using *N*-hydroxysulfosuccinimide (sulfo-NHS) and 1-ethyl-3(3-dimethylaminopropyl) carbodiimide hydrochloride (EDC) cross-linkers have been used to conjugate bovine serum albumin (BSA)/anti-BSA systems with green/red-emitting thioglycolic acid (TGA)-capped CdTe.[14] Silanized CdSe/ZnS nanoparticles with a thiolated surface were covalently bound to strands of oglionucleotides and deposited on prepared gold/silica substrates with complimentary DNA strands for color assortment DNA analysis.[12] Hydroxylated QDs were prepared with 1,1′-carbonyl diimidazole (CDI) for linkage to DNA and used in fluorescence in situ hybridization (FISH) experiments with human sperm cells.[15] The viability of QD bioconjugates for medical and biological applications is becoming well established, and their popularity is increasing in turn. Importantly, recent findings of acute toxicity in hepatocytes by CdSe without surface coatings highlights the need to properly condition the surface to be biocompatible and nontoxic.[16]

Silanization of various metal and semiconductor nanoparticle systems have shown great success in protecting their surface characteristics. Liz-Marzan et al. have grown a silica shell onto gold nanoparticles with controlled growth by initially priming

* Author to whom correspondence should be addressed. Phone: (831) 459-3776. E-mail: zhang@chemistry.ucsc.edu.
[†] University of California, Santa Cruz.
[‡] Lawrence Livermore National Laboratory.

10.1021/jp057435z CCC: $33.50
Published on Web 02/28/2006

the gold surface with (3-aminopropyl)-trimethoxysilane (APS) and growing the shell in ethanol using a modified Stöber method.[17] Growing silica shells around gold nanoparticles with adsorbed dye molecules was shown to be extremely effective as a surface enhanced Raman scattering (SERS) probe.[18] Others have used various procedures to grow silica shells to coat Ag, AgI, CdS CdSe, CdSe/ZnS,CdTe, CdTe nanowires, and CdSe/CdS.[6,19−24] During conjugation of bare CdTe nanoparticles to BSA, it was concluded that encapsulation was necessary to prevent particle growth, photoinduced decomposition, and conjugate aggregation.[13] Amorphous silica shells have been shown to provide some prime advantages necessary for bioconjugation of QDs. First, the silica shell prevents flocculation of particles, prevents species from adsorbing onto the surface, and helps to maintain the photoluminescence. Second, decoration of the silica shell with any number of functional groups including thiol, amine, phosphate, carboxylate, and poly(ethylene glycol) (PEG) groups allow for greater control in conjugation protocols. Water-soluble semiconductors (e.g., CdSe/CdS, CdTe) can benefit drastically through silanization by removing the dynamic stabilizer system (e.g., TGA) and replacing them with a permanent silica shell. Kirchner et al. reported high cell viability of various cell lines including MDA-MB-435S breast cancer and NRK cell lines when ingested and adsorbed with silica-coated CdSe/ZnS nanoparticles.[25] While mercaptopropionic acid (MPA)- and polymer-coated nanocrystals showed acute cytotoxic effects at 0.65 and 0.80 μM, respectively, silica-coated QDs showed no cytotoxic effects in the cell lines investigated with concentrations as high as 30 μM.[25] These results are confirmed by an analysis at the genetic level by probing the changes in the level of gene expression using a microarray with ~22 000 total probe sets, containing 18 400 probe sets from known genes.[26] Skin fibroblast cells transfected with high doses of silanized CdSe/ZnS show negligible changes in the gene expression level as compared to the same type of cells nonexposed to nanomaterials. Remarkably, silanized CdSe does not elicit genes related to exposure to heavy metals; this indicates that silica is an outstanding biocompatible protective layer and may hold the best promise for in vivo bioimaging. Recently, Kim et al. utilized near-infrared (NIR)-emitting CdTe/CdSe QDs for in vivo site-directed surgery. We believe exploiting CdTe NIR emission and the high biocompatibility of silica shells can provide a fantastic candidate for noncytotoxic bioimaging and site-directed surgeries.

In this work, we demonstrate the growth of an amorphous silica shell onto as-synthesized water-soluble CdTe QDs for the purpose of bioconjugation to immunoglobulin-G-type proteins. The QDs with and without silica shells have been characterized using spectroscopy and microscopy techniques. The QD/IgG bioconjugation was confirmed via agarose gel electrophoresis, commonly used in DNA analysis.[27] Water-soluble CdTe nanoparticles can be synthesized with many stabilizing agents such as TGA, mercaptoethylamine (MA), thioglycerol, and L-cysteine.[7] The quasi-shell of Cd−S on the surface is dynamic and is very sensitive to changes in pH and buffer solutions; both are prime disadvantages in performing conjugation of biomolecules. We found that as-prepared CdTe nanoparticles lose their highly fluorescent properties in the presence of common buffers such as phosphate-buffered saline (PBS) and Tris−borate−ethylenediaminetetraacetate (TBE). The growth of a silica shell has been found to significantly enhance the photoluminescence stability of CdTe QDs in buffer solution, provide a versatile platform for decoration with any number of functional groups and for successful conjugation to IgG proteins. Also, conjugation of our silanized QDs with streptavidin−maleimide with biotinylated polystyrene microspheres confirmed both bioactivity and binding specificity.

2. Experimental Section

A. Chemicals and Materials. Thioglycolic acid (TGA, T-3758), (3-mercaptopropyl) trimethoxysilane (MPS, M-1521), sodium silicate (27% SiO_2 in 14% NaOH, #338443), and 4-(*N*-maleimidomethyl)cyclohexane-1-carboxylic acid 3-sulfo-*N*-hydroxysuccinimide (sulfo-SMCC, M-6035) were purchased from Sigma-Aldrich (Milwaukee, WI). Aluminum telluride lumps (Al_2Te_3, A-1135) were purchased from Cerac, Inc. (Wilwaukee, WI). 2-[Methoxy(polyethylenoxy)propyl] trimethoxysilane (PEG-PS, SIM-6492.7) was purchased from Gelest, Inc. (Morrisville, PA). Cadmium perchlorate (99.999% purity, #44312), and sulfuric acid (1 N, #35655) were from Alfa-Aesar (Ward Hill, MA.) Sodium hydroxide (1 N, #SS266-1) was obtained from Fischer Scientific (Pittsburgh, PA).

Buffers used during agarose gel electrophoresis were 0.5× TBE made from Tris(hydroxymethyl)aminomethane (Tris base, molecular biology grade, BP-152-1), boric acid (electrophoresis grade, BP-168-500), ethylenediaminetetraacetate (EDTA, BP-121-500) from Fischer (Fair Lawn, NJ), and high-purity Milli-Q water (18 Ω). The 10× TBE buffer solution is created with 108 g of Tris base, 55 g of boric acid, 80 mL of 0.25 M EDTA, and 800 mL of Milli-Q water stored in autoclaved plastic bottles. Phosphate-buffered saline (10× PBS) contained sodium phosphate dibasic (Na_2HPO_4, S0876), sodium chloride (NaCl, S3014) from Sigma, potassium phosphate monobasic (KH_2PO_4, BP-362-500), and potassium chloride (KCl, BP-366-500) from Fischer. The 10× PBS procedure is 80 g of NaCl, 2 g of KH_2PO_4, 6.1 g of Na_2HPO_4, and 2 g of KCl in 1 L of Milli-Q water. SnakeSkin pleated dialysis tubing (10 kDa molecular weight cutoff (MWCO), #68100) was purchased from Pierce Biotechnology, Inc. (Rockford, IL). UltraPure agarose (15510-027) was purchased from Invitrogen (Carlsbad, CA). Agarose (BP160-500) low-EEO/multipurpose was purchased from Fischer Scientific. A horizontal gel electrophoresis minigel system (FB-SB-710) and FischerBiotech power supplies (FB300) were purchased from Fischer Scientific. The running buffer was 15% glycerol in 5× TBE buffer and 0.2 mM Arsenazo dye.

Mouse monoclonal immunoglobulin-type-G proteins (IgG), p-53 (sc-126), and ATF-2 (sc-242) were provided by Santa Cruz Biotechnology, Inc. (SCBT, Santa Cruz, CA). Polyclonal goat IgG Actin I-19 (sc-1616) and donkey anti-goat polyclonal IgG horseradish peroxidase (HRP) (sc-2020) were also provided by SCBT. Bovine anti-goat IgG HRP (sc-2350) was also provided courtesy of SCBT. Each primary antibody sample contained 200 μg of protein in 1 mL of PBS buffer with 0.1% sodium azide as a preservative and 0.1% gelatin for protein stabilization. The secondary antibody donkey anti-goat contains 0.6× PBS, 1% BSA, 0.02% thimerosal as a preservative, and 40% glycerol as a stabilizer. Streptavidin−maleimide (S9415) was purchased from Sigma Aldrich with an average molecular weight of 52 200 g/mol. FluoSpheres biotin-labeled microspheres (f-8769) were purchased from Invitrogen.

B. Synthesis of CdTe Nanocrystals. Thioglycolic-acid-capped CdTe nanoparticles were synthesized in the standard fashion from the literature.[7] Briefly, 0.985 g $Cd(ClO_4)_2 \cdot 6H_2O$ was dissolved in 125 mL of Milli-Q water, and 388.9 μL (5.7 mmol) of pure TGA was added. Dropwise addition of 1 N NaOH was then used to adjust the pH to 11.2−11.8 under vigorous stirring. After the proper pH is reached allow stirring to continue until the solution is optically clear. The cadmium

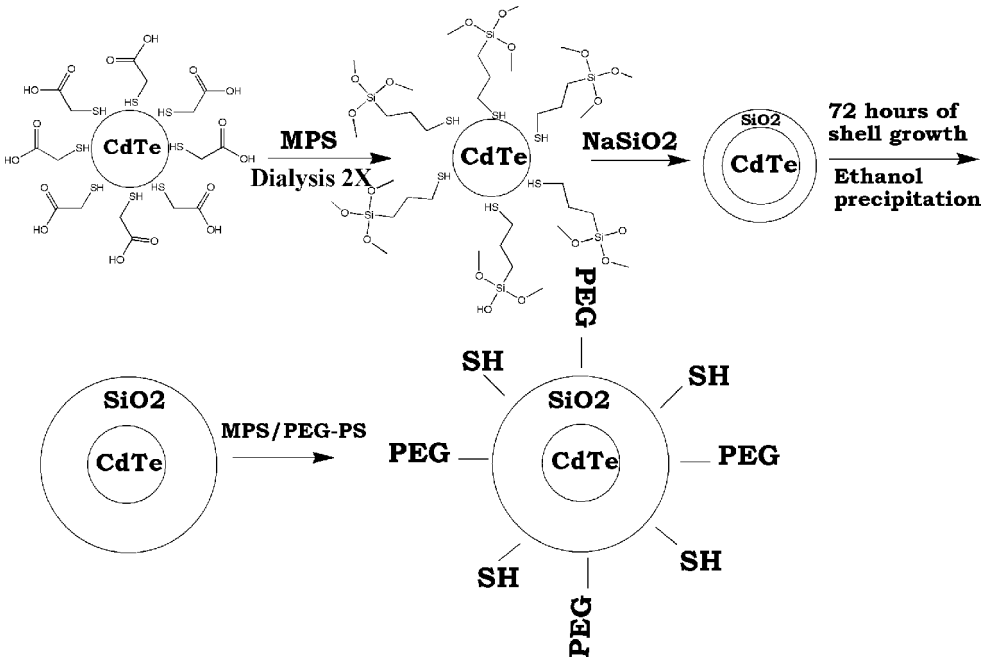

Figure 1. Schematic representation of silica shell growth on TGA-capped CdTe QDs through a modified Stöber method. Shell growth was accelerated rapidly by precipitating silica onto the already formed shell with ethanol. Functionalization of the surface with thiols and PEG groups allowed for bioconjugation using maleimide-containing cross-linkers and prevents nonspecific binding.

and thiol solution was placed in a 150 mL three-neck flask with rubber septums, a thermometer, and a large stirbar. Deaeration of the solution was performed under a robust flow of nitrogen with stirring at room temperature for 30 min. Next, 0.2 g (0.46 mmol) of Al_2Te_3 chunks were placed in a 50 mL three-neck flask fitted with an adjustable valve and septums in a nitrogen glovebox. Transfer of the flow of nitrogen through the small three-neck flask and into the larger three-neck flask containing the precursors are done quickly. Dropwise addition of 15−20 mL of concentrated sulfuric acid was then introduced to the Al_2Te_3 chunks to generate H_2Te and passed through the cadmium and thiol solution. At that time the solution changed from clear to a bright orange tone that is optically transparent. Nitrogen was passed through the solution for an additional 20 min at this point. A refluxing column with chilled water was then added to the 150 mL three-neck flask, and the solution was heated to 100 °C. CdTe nanoparticle growth begins during the refluxing and can be monitored using UV−vis absorption and photoluminescence (PL) spectrometry (Figure 3). Aliquots of 8−10 mL were then removed periodically from 1 to 42 h of refluxing from the crude solution of CdTe nanoparticles. Samples were stored in the dark at room temperature in scintillation vials with no other additional precautions.

C. Silanization of CdTe Nanocrystals. To 1 mL of as-prepared crude TGA-capped CdTe nanoparticles, 150 μL of MPS (48 mM in pure ethanol) was added. To ensure even distribution of MPS, a mini-stirbar was utilized during the 1−2 h required for surface priming. If mini-stirbars are not available, occasional vortexing can also be implemented to facilitate better stabilizer exchange. Next, the entire solution was placed into dialysis tubing and dialyzed versus 2 L of basified Milli-Q water at pH 11 for approximately 1 h. To assure complete surface coverage, an additional 150 μL of the MPS solution was added and dialysis was continued for another hour. After surface priming, 200 μL of sodium silicate was added to the solution under stirring to initiate silica polymerization at the particle surface. This slow shell growth was continued for 72 h to ensure even growth around the CdTe QDs.[17] To facilitate thicker silica shells, 300−400 μL of pure ethanol was added to decrease silicate solubility and then vortexed to ensure proper mixing. Smaller particles (2.0−3.0 nm) tend to need less ethanol to force the precipitation of the particles out of solution. Larger particles (3.0−6.0 nm) took larger quantities of ethanol and increased time until turbidity is apparent. The solution was slightly turbid and the color of the precipitate was consistent with that of the solution before precipitation. The precipitated CdTe nanoparticles were centrifuged at 13 000 rpm for 2 min, and the supernatant was discarded. The QD pellet was redispersed in 1 mL of Milli-Q water and then sonicated for 30 min in Eppendorf tubes. Particles quickly reentered solution with no change in color, clarity, or optical properties. Next, to functionalize the surface of the silanized QDs, 85 μL of MPS (48 mM) and 40 μL of PEG-PS (18 mM) were added and allowed to react for 24−48 h (Figure 1).

D. Photophysical Characterization. All UV−vis spectra were recorded on a Hewlett-Packard 8452A diode array spectrophotometer (Palo Alto, CA). Photoluminescence spectra were gathered on a Perkin-Elmer LS 50B (Fremont, CA) with an excitation wavelength of 390 nm and 1% attenuator. Samples were placed in an open-sided 1-cm-path-length quartz cuvette for both PL and UV−vis measurements.

The PL stabilities of the silanized QDs in both 0.5× TBE and 1× PBS buffer were also determined on a Perkin-Elmer LS50B in time drive mode. Approximately 50 μL of the silanized QDs were diluted with 2 mL of either TBE or PBS buffer, mixed, and then immediately placed in the cuvette holder. Excitation was set at 390 nm, and the probing of emission was done at various wavelengths, depending on the size of the particle investigated, and ran for 1−2 h. Pure as-synthesized QDs were also placed in the buffer solutions with the above procedure.

E. Size Characterization. The size determination of CdTe nanocrystals was performed using a high-resolution transmission electron microscope (TEM-CM200FEG at 200 keV). Samples of 10 μL drop dispersions were placed on Lacey Formvar 300 mesh copper carbon-coated grids and allowed to air-dry. The setup includes a Phillip double tilt background holder and Gatan imaging filter with a charge coupled device (CCD) camera and

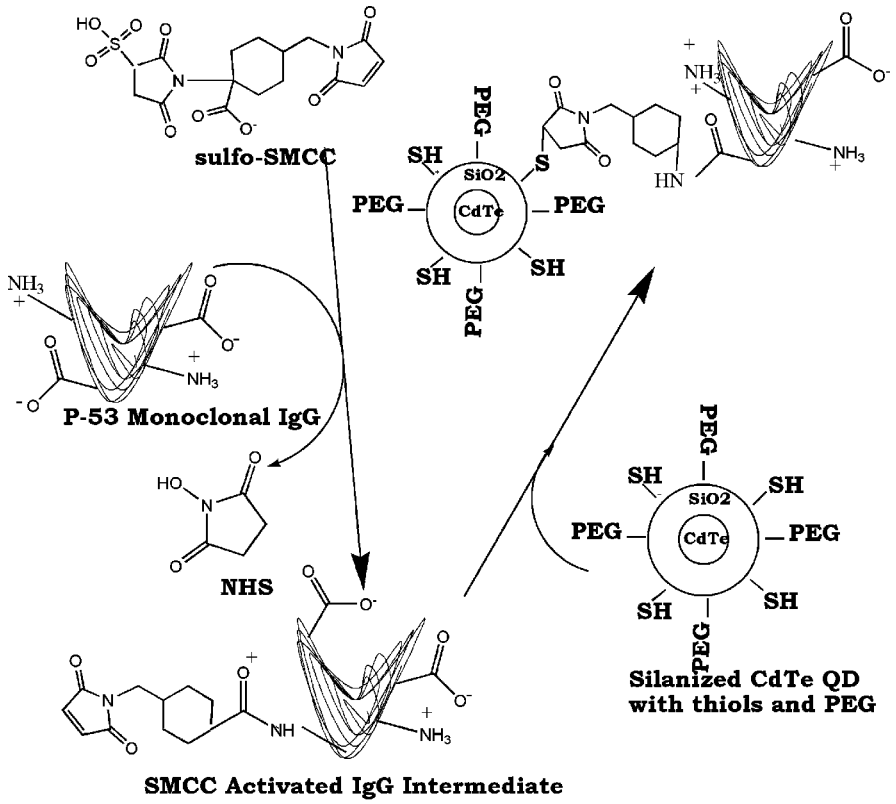

Figure 2. Schematic illustration of the bioconjuagtion of monoclonal antibodies and thiolated CdTe QDs. Sulfo-SMCC reacts to form amide bonds with the protein, and NHS is the leaving group. The active intermediate contains a stable maleimide group to covalently bond with the QD system. PEG groups are added to ensure that nonspecific binding is prevented between the QDs and the inactivated proteins.

an energy resolution of 0.9 eV and a spatial resolution of 1 nm. Images were analyzed using Digital Micrograph software, also from Gatan.

Additional size information was collected using atomic force microscopy (AFM). The atomic force microscopy measurements were conducted on a Pico LE SPM microscope (Molecular Imaging, Phoenix, AZ) using silica-etched tips. Typical samples were investigated at scan rates of 1−3 Hz with 256 × 256 pixel resolution during image capturing. Samples were dropped onto a stripped graphite sheet, and argon was lightly blown over the surface to disperse the particles evenly. Measurements were taken in tapping mode in air. Size determination was performed by individually recording the *z*-axis height of each particle and subtracting the surrounding *z*-axis graphite sheet height. A total of 200 particles were used to determine the size distribution of both the pure and the silanized CdTe samples.

F. Bioconjugation Protocol. Approximately 300 μL of monoclonal antibodies as provided was activated with 100 μL of hetero-bifunctional cross-linker sulfo-SMCC (3.34 mM) at room temperature in Eppendorf tubes and allowed to react for 1−2 h. Approximately 30 μL of silanized QDs were then added to the activated cross-linker/protein system and stored in a fridge for 24 h (Figure 2). The 1% agarose gels were prepared in 0.5× TBE buffer and solidified in a 4 °C cold room. Approximately 30 μL of as-prepared bioconjugates and 10 μL of running buffer were mixed, vortexed, and added to the wells. Common gel runs had voltages ranging from 75 to 150 V and were run typically for 5−20 min. Illumination of the gels was performed with a Fischer Biotech transilluminator FBTIV-88 UV lamp and model DC290 digital Kodak camera using Kodak one-dimensional imaging software.

Streptavidin−maleimide and biotinylated microbeads were conjugated with silanized CdTe as follows. Approximately 1.1 mg of Streptavidin−maleimide was dissolved in 100 μL of PB buffer (10 mM), vortexed, and then sonicated to ensure complete solubilization. Approximately 10 μL of the streptavidin−maleimide (210.7 μM) solution was then added to 45 μL of as-prepared silanized QDs (10:1 molar ratio), vortexed, and allowed to sit for 1 h. The biotinylated silica microbeads were first transferred into PB buffer by adding 15 μL of the microbeads with 20 μL of PB buffer and centrifuging the solution. The supernatant was removed, and the washing procedure was performed twice more. The pellet was redispersed in 20 μL of PB buffer, 5 μL of the streptavidin−maleimide−QD bioconjugate was added and vortexed, then allowed to react for 30 min. To remove any unconjugated material from the microbead system several washes with PB buffer were performed, and the pellet was redispersed into Milli-Q water for imaging. A glass slide was cleaned with ethanol, heated to 50 °C, cooled, and 5 μL of the microbead solution was dropped onto the slide. The collection of microbeads was visualized under white light and then illuminated by a UV source and recorded.

3. Results

A. Photophysical Properties. The absorption and emission spectra of as-synthesized CdTe QDs in Milli-Q water are shown in Figure 3. The UV−vis absorption spectrum shows the characteristic electron−hole pair (exitonic) peak representative of the band gap energy. The exitonic peak positions shift to longer wavelengths as the QD ensemble grows to larger diameters. During the growth of the particles, smaller particles will dissolve and become the constituents of larger particles, a process known as Ostwald ripening.[28] An effect of the Ostwald ripening is the increase in size distribution, a phenomenon termed "defocusing". This effect is seen clearly in the "flattening" of the exitonic peak as particles increase in size during

Figure 3. UV−vis and PL spectra of CdTe QDs capped with TGA in aqueous solution. The spectra were taken from aliquots taken from 1 to 42 h of refluxing. The exitonic peak position and emission spectra allow for monitoring of particle growth.

the growth phase. Narrow size distributions are reflected in a very sharp exitonic absorption peak.[5]

The PL spectra of as-synthesized CdTe reveal the tunable emission spectra in the visible range. Each emission spectrum corresponds to an aliquot of particles taken out of the reaction vessel during the growth phase. Particles in the 2 nm range were removed first and due to their small diameter have emission peaks in the blue-shifted wavelength region. This particular batch of QDs show emission peaks from 530 to 630 nm after refluxing times of 1−42 h. The size-dependent quantum confinement effects are apparent during the growth process as aliquots in scintillation vials shift across the visible spectrum from green to red emission (Figure 3, inset). Two distinct features in the emission spectra are worth elucidating upon. First, the PL efficiency was dependent upon the aliquot taken and peaked in quantum yield when 6 h of refluxing had occurred. Talapin et al. have given an in depth explanation of this PL effect for CdSe, CdTe, and InAs based upon growth rates of the ensemble of QDs.[29] Second, the emission band becomes broader during the continued growth. The full width half-maximum (fwhm) of the emission spectrum after 1 h of refluxing is 35 nm (0.119 eV) but slowly increases to 55 nm (0.181 eV) during the course of the growth phase after 42 h. This again is an effect of the Ostwald ripening mechanism as smaller particles dissolve in the process of creating larger particles and results in a broader distribution in particle size. The PL band fwhm provided an estimate of the general size distribution during growth.

The PL spectra show the characteristics of high-quality CdTe nanoparticles with a well pronounced band gap emission and no trap state emission. Occasionally, aliquots during the growth process will exhibit a strong band edge and some shallow trap state emission. The effect of silanization on trap state emission will be discussed shortly. Crystal growth is slow compared to high-temperature solvents (e.g., TOPO), and tracking of the growth process was controlled and monitored easily. The quantum yield of the as-prepared QDs are 8−10% in comparison to rhodamine 6G in ethanol, with 0.1 optical density used at the excitation wavelength for the PL measurements.[30] This quantum yield is much higher than the ones typically obtained from CdSe nanocrystals prior to the inorganic ZnS or CdS shell growth.

Comparison of the PL spectra before and after the silanization process reveals the removal of shallow trap states from the QD surface for samples that do show trap state emission before silanization. For example, as shown in Figure 4, a particular aliquot after 5 h of refluxing showed a strong shallow trap state

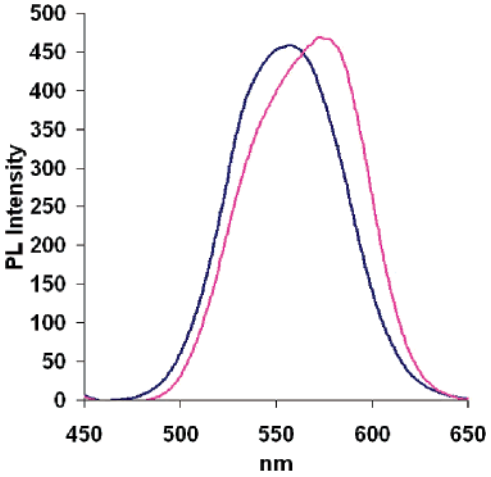

Figure 4. Photoluminescence spectra of the same sample of CdTe before and after silanization. The as-synthesized CdTe QD sample has a shoulder at the band edge emission at 555 nm and a pronounced shallow trap state at 580 nm (right). After silanization, the passivation of the surface reduced the trap state emission, and the band edge emission became more dominate. This is mainly attributed to the exchange of ligands from TGA to MPS and the decrease in charged species on the surface.

emission at 580 nm, near the pronounced band edge emission at 550 nm. After silanization, the band edge emission became dominant while the trap state emission largely disappeared. The PL intensity of solutions of silica-coated QDs after silanization and ethanol precipitation was tested in both PBS and TBE buffers (Figure 5A). Figure 5A shows fluorescence quenching within 15 min of silanized QDs after ethanol precipitation in buffers and gradual leveling of the PL after 30 min. The PL studies of as-synthesized CdTe, silanized CdTe without ethanol precipitation, and silanized CdTe revealed significant fluorescent quenching in 0.5× TBE buffer (Figure 5B). Figure 5B depicts the quick quenching of both as-synthesized and thinly shelled QDs within 5−10 min while thickly shelled QDs resisted quenching. It was observed that the thickening of the silica shell had dramatic effects in the stability of the luminescent properties compared to those of unsilanized CdTe and thinly shelled CdTe. It is worth noting here that amorphous silica plays a role similar to that of epitaxially grown ZnS or CdS shells around CdSe cores. These inorganic shells increase the QY of the cores and protect their photostability at appropriate shell thicknesses.

B. Size Characterization. High-resolution transmission electron microscopy (HRTEM) and AFM data provide informa-

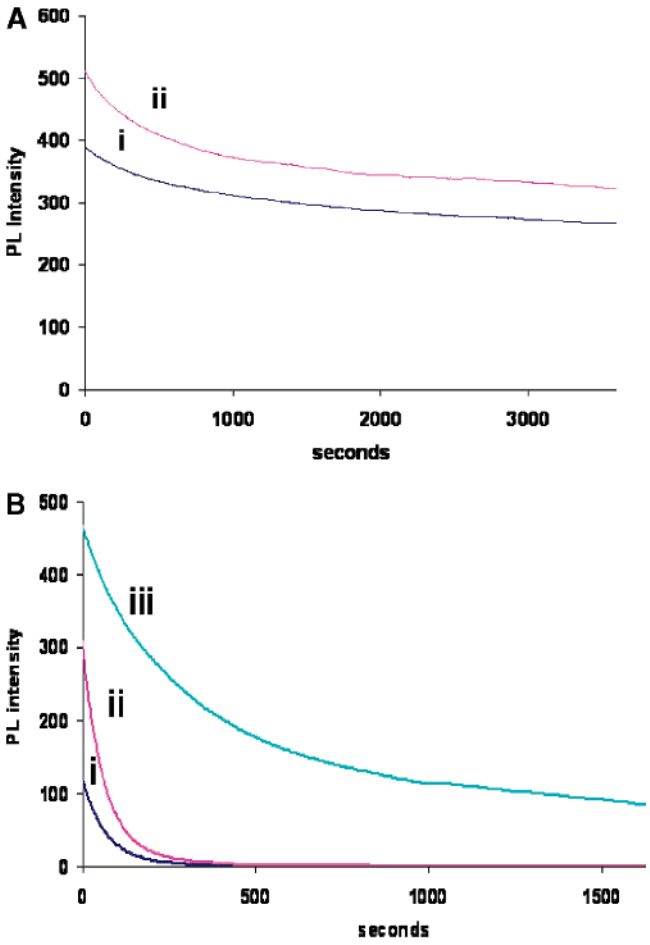

Figure 5. Photoluminescence data taken at the emission peak of silanized QDs in biological buffer solutions. Excitation was set at 390 nm, the sample was probed at an emission wavelength of 551 nm, and a 1% attenuator was used. (A) Photoluminescence spectra of silanized CdTe nanocrystals over a period of 2 h in PBS (1×) buffer (ii) and TBE (0.5×) buffer (i). (B) Photoluminescence spectra in TBE (0.5×) buffer of thick-shell silanized CdTe QDs (iii), thin-shell silanized CdTe QDs (ii), and as-synthesized CdTe capped with TGA (i). Notice the significant PL intensity drop when only the initial SiO_2 growth is allowed to proceed without the precipitation step. After the ethanol precipitation and thicker shell growth, a vast improvement in PL intensity was observed.

tion about the size of CdTe nanoparticles and silica shell thickness. Atomic force microscopy data taken of as-prepared QDs and silanized QDs allow the average shell thickness to be determined. The particle size was calculated individually by measuring the *z*-axis height of an imaged particle and subtracting the surrounding graphite sheet *z*-axis height. As-synthesized QDs show a size distribution from 2 to 8 nm with an average of approximately 4 nm, while silica-coated QDs show a size distribution of 4−16 nm with an average size of 10 nm (Figure 6). Unsilanized QDs show a population clustering from 2 to 3 nm in diameter, and it trails sharply down with nanoparticles in the 4−8 nm range. Silanized QDs show a spattering of particles from 3 to 7 nm in diameter and a dramatic increase in the number of 8−10 nm QDs with a tailing population from 11 to 16 nm similar to the trend seen with bare nanocrystals. Representative three-dimensional AFM images of uncoated and coated QDs are shown in Figure 7. Silanized CdTe exhibited a pattern on the substrate that suggests a good dispersion of the particles and negligible aggregation. The distribution of heights of silica-coated CdTe may indicate a wide range of silica shell thicknesses. However, it has to be viewed in conjunction with

Figure 6. Size distribution of as-synthesized CdTe QDs (blue) and silica-coated CdTe QDs functionalized with thiols and PEG (red). Measurements were taken along the *z*-axis of the raw AFM data by taking the overall *z*-axis height and subtracting the surrounding base height. Those particles believed to have been cross-linked or aggregated were omitted from the overall size distribution and considered outliers.

the relatively large distribution of sizes in CdTe cores. An explanation, supported by our previous study on silanized CdSe, is that smaller cores are coated with thinner silica shells than bigger cores.[6] Thus, if a 3 nm CdTe core is embedded into a 1.5-nm-thick silica shell (total particle size 6 nm), a 6 nm CdTe could be embedded into a 3 nm silica shell (total particle size about 12 nm). Notice however that the overall size of the silica-coated CdTe particles remains considerably smaller than commercially available QDs embedded in a polymer shell.[31] There may be other contributions to the observed height distribution. Aggregated particles that exhibited unusually large sizes were not included in the QD population. Upon the basis of the exitonic peak position of 525 nm, an experimental data fitting polynomial predicted a size of 2.89 nm for CdTe nanocrystals.[32] The observed average particle size of ∼4 nm is larger than that predicted based on the exiton position, which could be due to a passivating shell of CdO, the stabilizing molecule TGA, or a tip effect that distorted the *z*-axis measurements.

Figure 8 shows a representative HRTEM image of CdTe QDs with a well-resolved 6 nm nanocrystal next to an amorphous silica particle of approximately 3 nm. The silica shell was not well resolved in the HRTEM images, and thus AFM was needed to effectively characterize the shell thickness. With the average shell thickness of 2−5 nm, AFM was able to provide a good estimate. Previous studies on the silica coating of CdSe/ZnS QDs indicate that the silica shell may be as thin as 2 nm and amorphous. Our current study using AFM also supports the fact the silica shell is a few nanometers thick. In addition, both Si and O are light atoms and provide weak scattering for the electron beam in transmission electron microscopy (TEM). The consequence is that the silica shell is not clearly discernible in a TEM or HRTEM study. Therefore, the morphology of the silica shell has been inferred through indirect approaches such as AFM.

C. Surface, Shell Growth, and Bioconjugation Characterization. The surface charge and shell growth of the silanized QDs were investigated by agarose gel electrophoresis. Agarose gel electrophoresis is a common tool for separation and purification of DNA fragments.[33] Migration through the gel matrix is dependent on the size and surface charge of the particles of interest and is driven by electrostatic forces.[34] Silanized QDs with hydroxyl groups on the surface gave an average negative charge; thus particles run toward the positive node of the gel setup. Surface hydroxyl groups are a relic of the silanization and functionalization steps. MPS molecules may randomly orient on the QD surface, and methoxy groups then become hydrolyzed in solution and face outward into the solution.[6] For polymerization to occur, two MPS molecules have

Figure 7. Three-dimensional AFM image of both as-synthesized and silanized CdTe QDs taken in tapping mode with silica-etched tips. The scan rates were from 1 to 3 Hz with 256 × 256 pixel resolution of a 2 × 2 μm^2 area. Silanized QDs separate well on the graphite sheet and show few signs of aggregation.

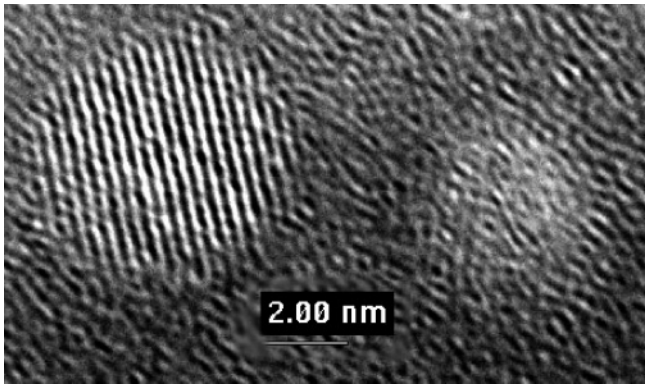

Figure 8. Representative high-resolution transmission electron microscopy image of a 6 nm CdTe nanoparticle, with an amorphous silica particle to the right. The lattice spacing was calculated to be 0.159 nm (1.59 Å) on average.

to come in close proximity and react. The likelihood of such an event is increased if one of the two molecules becomes immobilized. This is a process similar to a seeded growth. Therefore, we expect that polymerization of MPS will occur more rapidly onto a CdTe seed. Thus free MPS polymerization in solution is limited but cannot be completely eliminated.

Figure 9 (top panels) shows a common 1% agarose gel run with 0.5× TBE running buffer. Gradual quenching of the silanized nanoparticles was observed while silanized CdSe/ZnS synthesized by known literature methods were the control.[6] Bioconjugates in that particular gel were of thin-shelled CdTe QDs and had not been subjected to ethanol precipitation. The quenching was highly reproducible from silanized sample to sample and showed the need to thicken the silica shell. After the ethanol precipitation, bioconjugates and silanized QDs remained highly fluorescent during the gel electrophoresis runs (Figure 9, bottom panel). Notably, the largest particle sample of CdTe with a refluxing time of 42 h was unable to penetrate into the gel matrix after the ethanol precipitation step (Figure 9, well C, bottom panel). Interestingly, this provided an estimated nanoparticle size cutoff for QD movement into the agarose gel matrix. Later, silanized samples of smaller diameter CdTe nanocrystals were tested to clearly delineate between bioconjugate confirmation and QD movement in gel runs. The limited fluorescence of the immobile bioconjugates in wells may be due to extra charge on the QD surface in 0.5× TBE buffer and will be described below. Quantum dots in the matrix showed a drastic enhancement in fluorescence that we attribute to the reduction of charged species transported through the amorphous silica shell and onto the particle surface.

Bioconjugates of various IgG proteins and silanized CdTe nanoparticles were unable to penetrate into the gel matrix. Thinly shelled QDs conjugated to polyclonal IgG sc-2350 were retarded in their movement while unconjugated QDs quickly passed into the agarose (Figure 9, top panels). Upon close inspection a very faint QD front is seen in front of the bioconjugate well and fades quickly in the procession of images. Its movement is dramatically less than that of its unconjugated silanized CdTe counterpart. All bioconjugates whether thin or thickly shelled and conjugated to either monoclonal or polyclonal antibodies were immobile in the agarose matrix.

Agarose gel electrophoresis provided a quick and reproducible platform to check if a silica shell had in fact been grown. An increase in particle size slowed the particle speed, and one can easily differentiate between silanized and unsilanized QDs in an agarose gel (Figure 10). Those silanized particles in Figure 9 (top panels) were not yet subjected to the ethanol precipitation and thus had thinner shells that were never hindered in their movement into the gel. Comparison of Figure 10 (well D) with Figure 9 (well C, bottom panel) clearly shows the size increase before and after the precipitation step of the largest sample of CdTe (42 h of reflux). Figure 10 (well D) shows penetration into the gel with smearing of the band while Figure 9 (well C, bottom panel) does not penetrate and remains significantly less luminescent within the well.

4. Discussion

A. Synthesis and Silanization. As discussed in the introduction, silanization techniques have been exploited for many systems of metals and semiconductor nanoparticles. Ströber's method, which has been modified for various applications, is based on the formation of SiO_2 spheres by condensation reactions of tetraethoxysilane in basic conditions.[35] Silica coatings have proved to be effective at preserving optical properties and preventing precipitation for organometallically

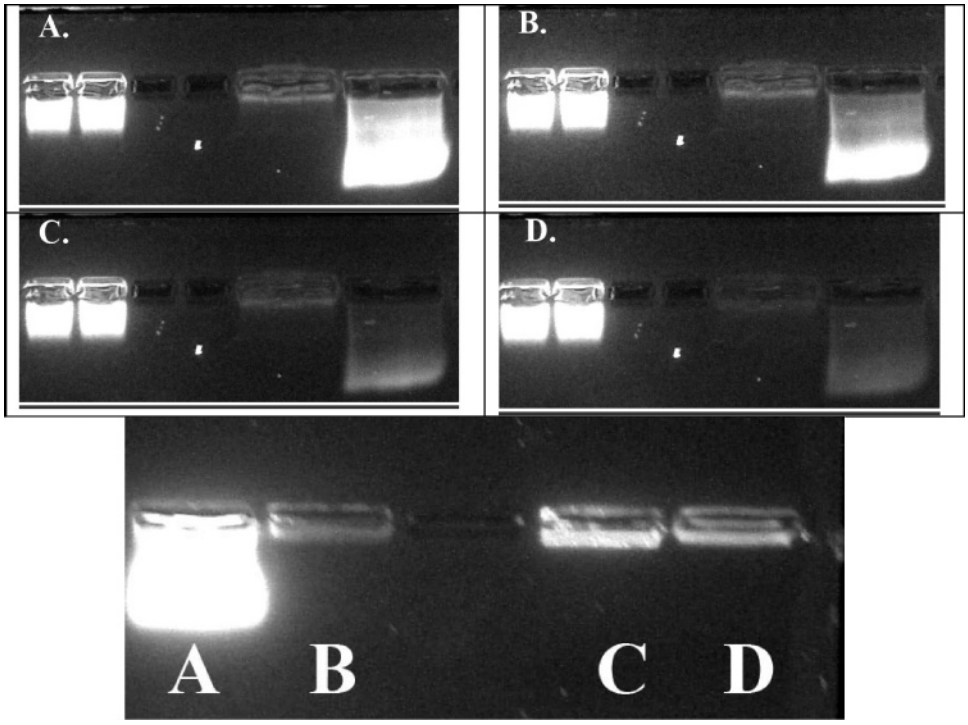

Figure 9. Agarose gel electrophoresis (1%) in 0.5× TBE before (top panels) and after (bottom panel) ethanol precipitation of silanized CdTe QDs and bioconjugates. Images A−D (top panels) include a progression of images of silanized CdSe/ZnS as a control on the left and thinly shelled CdTe and CdTe/IgG sc-2350 bioconjugate on the right. The PL quenching is blaringly apparent from images A−D taken 3 min after one another. The bottom image of wells A and B are thick-silica-coated CdTe (8 h of reflux) and bioconjugates of the same CdTe sample with protein ATF-2. Wells C and D are silanized CdTe (42 h of reflux) and bioconjuagtes of the same sample of CdTe with ATF-2. The silanized CdTe of both 8 and 42 h of reflux had ethanol precipitation performed to thicken the shell. Notice the drastic increase in PL before and after the ethanol precipitation. Well C, which included the largest of all silanized samples, did not move into the gel matrix due to its large size (∼15 nm) and was considered a good marker for particle size cutoff. Bioconjugates consistently showed their inability to move into the gel matrix after conjugation to the proteins.

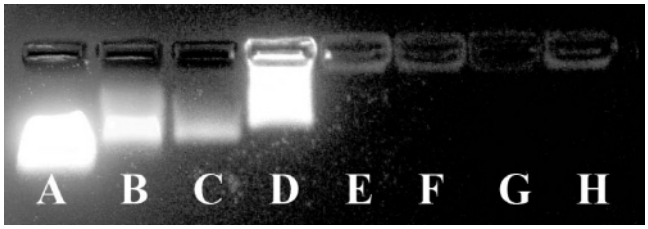

Figure 10. Various QD samples and bioconjugates in an agarose gel, run for 7 min at 100 V in 0.5× TBE buffer. Samples include wells A and B, unsilanized CdTe QDs (∼3 nm, 5 h of reflux) and silanized QDs from the same synthesis aliquot. Wells C and D are unsilanized CdTe (5−6 nm, 42 h of reflux) and its silanized counterpart as well. Importantly, these samples had yet to have been precipitated with ethanol and thus had a thinner shell. Compare well C of Figure 9 versus well D of Figure 10 to see the difference in QD movement before and after ethanol precipitation. Wells E and F are bioconjugates of IgG sc-2350 (SCBT, Santa Cruz, CA) with silanized CdTe functionalized with thiols and PEG. Wells G and H are bioconjugates of IgG sc-2020 with silanized CdSe/ZnS QDs functionalized with thiols and PEG as a control.

prepared nanocrystals.[6] Silica growth on the surface of CdTe in this instance was specifically done to decrease fluorescence quenching in biological buffers, create a platform to modify the surface, and enhance the biocompatibility of the nanocrystals.

The ease of synthesis of CdTe in aqueous solution and the ability to track growth and remove sizable aliquots during the growth stage is highly advantageous.[7] It is also possible to narrow the size distributions using size-selective precipitation for as-synthesized aqueous QDs.[36] The use of basified dialysis during the ligand exchange process has dual benefits in that excess reactive precursors (TGA, Cd^{2+}) are removed, and it advances the priming of MPS onto the QD surface. Aliquots of crude solution typically have strong band edge emission, were stable for 6−12 months, and have reasonably high quantum yields (8−10% with TGA capping agent). The growth of a silica shell under these conditions allowed for high reproducibility, simpler steps for silanization in comparison to organometallic QD silica shells, an ability to increase batch sizes, and a biocompatible system that can be utilized immediately. Aqueous semiconductor synthesis does have its disadvantages in size distribution broadening and lower crystallinity than organometallic routes.[29] We feel that those disadvantages are outweighed significantly by the simplicity afforded in aqueous synthesis and subsequent silanization.

Our silanization process is straightforward (Figure 1) and begins with the ligand exchange of TGA with MPS molecules. This priming step is believed to be the most crucial to ensuring homogeneous shell growth. Early attempts of priming the surface without dialysis concluded with incomplete shell growth, which was attributed to the lack of complete coverage of MPS on the CdTe surface. Dialysis kinetically pushes the removal of TGA off the particle surface and into solution while the excess MPS coats the particle surface. Excess dialysis was also found to be problematic, with flocculation occurring due to removal of too many capping molecules from the surface. Proper dialysis time is quantitative at best and may differ from batch to batch. We found that 1 h of dialysis was sufficient and produced good results while dialysis on the order of 4 h was excessive. Polymerization of the shell must be performed at high pH (∼11) to activate the sodium silicate after dialysis is performed, so basification of the dialysis was required.

Thin shells grown on the QDs alone were insufficient to protect fluorescent properties in biological buffers (Figure 5B). Ethanol precipitation was used to crash unpolymerized SiO_2 onto

to the already grown shell and speed up growth. Redispensing of the silanized QDs back into solution was done through sonification, and the color, clarity, and optical properties remained identical. Some aliquots removed from the crude solution had both band edge and shallow trap state emission prior to silanization. After silanization, the passivation of the surface had occurred during shell growth, and pure bandedge emission was regained with trap state emission removed (Figure 4).

Photoluminescence studies of as-synthesized crude particles and thin-silica-shelled and thick-silica-shelled CdTe nanoparticles were investigated in biological buffers (Figure 5). The stability of silanized CdTe nanoparticles in TBE and PBS buffers was discovered to be a function of shell coverage and thickness. Crude CdTe solutions were found in both TBE and PBS buffers to quench within 5−10 min and subsequently flocculate to a brown-red bulk material. Fluorescence and UV−vis showed the elimination of both bandedge emission and exitonic absorption (not shown). This indicates that fluorescence quenching is likely connected with a chemical transformation of the underlying CdTe cores. QDs with 72 h of silica shell growth performed slightly better than crude nanocrystals but not significantly (Figure 5B). We attribute this to both inhomogeneous silica shell growth around the particle surface and the amorphous nature of the shell, which permits the transport of ionic quenching species to the surface. Unlike the crude solution, however, they retained their original color and were optically clear. UV−vis absorption confirmed that the nanocrystals were still displaying normal exitonic behavior (not shown). This confirmed that interactions between particles was mediated by the shell; the silica shell prevented flocculation and kept the structural integrity of the CdTe cores but was insufficient for fluorescent stability.

Ethanol precipitation of silica on to the already formed shell proved to more effectively reduce fluorescence quenching. The growth of the silica shell, which was found to be 2−5 nm thick, showed drastic improvement over thinly shelled silanized QDs. In both TBE and PBS buffers, a noticeable quenching did occur but did reach an equilibrium state after 2−3 h and would remain fluorescent but with 50% of the initial fluorescence intensity (Figure 5A). Again we believe this quenching to be due to the amorphous nature of the silica shell and access of ions to the surface. Yet the access is presumed to be far less than what was seen without the ethanol precipitation. Further advancements in the priming step with MPS and the addition of sodium silicate may further reduce the quenching phenomenon and lead to more PL stable QDs in buffer solution. A possible alternative approach to maintain CdTe brightness is to grow a thin shell of CdSe between the CdTe core and the silica shell. Although we did not perform this additional step in this study, we feel confident that such step is a straightforward extension of our current protocol. Silica-coated CdTe core samples were shown to remain fluorescent after conjugation in a streptavidin−maleimide/biotinylated polystyrene microsphere system and will be discussed below.

B. Bioconjugation and Bioactivity. Preparation of the silica shell and its subsequent thiol decoration was specifically created for use with the hetero-bifunctional cross-linker sulfo-SMCC. LC-SMCC and its sulfonated analogue, sulfo-SMCC, have been widely used as conjugation agents for protein−protein and protein−molecule purposes.[37] Kitagawa et al. employed the sulfhydryl reactive maleimide group to conjugate insulin and β-D-galactosidase and found that bioactivity remained high.[38] The reactive sulfo-NHS group creates amide bonds between the IgG and the cross-linker and leaves a long-lived maleimide reactive intermediate (Figure 2). The cyclohexane ring in sulfo-SMCC stabilizes the maleimide group and was found to be 50% stable in PB buffer after 64 h.[37] Here we have modified that protocol to allow our thiolated QDs to be easily and efficiently conjugated to IgG proteins and streptavidin−maleimide for interaction with polystyrene biotinylated microspheres.

Agarose gel electrophoresis was used to confirm that bioconjugation between the IgG proteins and QDs were successful. Agarose gels are easily prepared in minutes and remove much of the time-consuming work associated with confirming bioconjugation using sodium dodecyl sulfate polyacrylamide gel electrophoresis (SDS-PAGE).[14] Another advantage is the lack of ethidium bromide in the agarose gel preparation, thus allowing for easier handling. Quenching of the silanized QDs and bioconjugates immediately showed the need to strengthen the ability of the QDs to fluoresce in both the TBE buffer and the gel matrix (Figure 9, top panels). Unexpectedly, it also revealed the inability of the bioconjugates to enter into the gel matrix (Figures 9 and 10). Kim et al. recently saw a similar trend with poly(L-lactic acid) and poly(D,L-lactide-*co*-glycolide) nanoparticles conjugated to pDNA that was immobilized and also did not enter into the gel matrix.[39] This retardation in movement has two valid explanations. One is that the charged QDs conjugated to the noncharged protein lack sufficient charge density to allow the bioconjugate to efficiently move into the gel at 100 V (i.e., about 16V/cm). The other is that the orientation and size of the bioconjugate is simply too large to move through the matrix. In our case, repeated gel runs consistently showed that silanized QDs could enter into the gel matrix except for the largest (42 h reflux) of the thickly shelled QDs (Figure 10, well C). This indicates that a QD molecular weight cutoff exists that has been not fully clarified qualitatively. After conjugation we did not observe any noticeable amount of unconjugated QDs moving into the gel matrix. The conclusion from the observation is that the bioconjugation protocol utilizing sulfo-SMCC was efficient.

Bioactivity and specificity after conjugation was confirmed using streptavidin−maleimide and biotinylated polystyrene microspheres. The strong interaction between streptavidin and biotin has been well-known as a tool to improve immunofluorescence and enyzme-linked immunofluorescence assays (ELISA).[40] Activation of the streptavidin with the QDs was through the suflhydryl reaction-specific maleimide group. Binding specificity was aided by the decoration of PEG groups onto the QD surface to prevent nonspecific binding from occurring.[41,42] Biotinylated microspheres and the streptavidin/QD system were washed multiple times to remove unconjugated material and showed superb binding characteristics (Figure 11). Cavities in the microsphere deposition directly correlate to the lack of fluorescence under UV illumination in those same areas and with exactly the same size and shape. The QDs were highly fluorescent and remained fairly fluorescent on the glass slide surface when visualized a month after the original conjugation occurred (not shown).

C. Quantum Dot Silica Shell Characterization. Amorphous silica shell growth was found through AFM measurements to be from 2 to 5 nm in thickness on the surface of the CdTe nanoparticles. Figure 6 shows two general peaks for both the as-synthesized QDs and the silanized QDs. For the as-synthesized QDs, the particles show the two peaks at 3 and 6 nm in diameter, while the two peaks of the silanized QDs are at 9 and 12 nm. This correlation in the QD diameter shift of 6 nm could be strong evidence for a generally uniform shell growth, with the final diameter mainly dependent on the initial

Figure 11. Streptavidin−QD−biotinylated microbead pictures under white light (left) and UV illumination (right) on an ethanol-cleaned glass slide. Portions of the left image show areas of no microbead coverage, and this lack of fluorescence is easily seen in gaps of the exact size and shape under UV illumination. No errant QDs were found, and we have confirmed the biospecificity of the bioconjugation protocol.

CdTe core size. In the first report of silica shell growth around CdSe/ZnS QDs, it was suggested that the silica shell thickness around 4 nm nanocrystals was 1−2 nm, while its thickness around 6−7 nm QDs was 3−4 nm.[6] This interpretation is consistent with further fluorescence correlation spectroscopy (FCS) measurements that indicate that the hydrodynamic radius of silanized CdSe/ZnS QDs is dependent on the initial size of the underlying quantum dots. The same trend could be observed in the case of CdTe quantum dots. Finally, on the smaller side of the histogram distribution in Figure 6, i.e., particles in the 3−7 nm regime, one can be attributed to either pure amorphous silica spheres or CdTe nanoparticles that grew a thin shell or failed to grow a silica shell at all. The evidence would support the former case of silica spheres forming, which was also observed by Rogach et al. using a similar protocol.[20] Failure to perform the basification of the solution of dialyzed QDs prior to sodium silicate addition resulted in little to no silica shell growth and a quenching of fluorescence in buffers. Ethanol precipitation provided the necessary tool to quickly thicken the shell and protect PL characteristics.

5. Conclusion

Silica shells were grown on water-soluble CdTe QDs, and the surface was decorated with thiol and PEG groups for use in bioconjugation. The silanization protocol is straightforward, and the use of dialysis to push the ligand exchange of TGA to MPS was found to be highly advantageous. Atomic force microscopy data show the growth of 2−5 nm thick shells onto the surface. Shallow trap states of as-synthesized silanized QDs were removed during silanization while band edge emission remained. With silanization, the overall PL quenching was reduced in TBE and PBS buffers and was found to reach an equilibrium state after 2−3 h. The growth of a thick silica shell after initial growth was found to be essential via an ethanol precipitation step and allowed for easy redispensing back into solution. Exploitation of the thiol-decorated surface with the hetero-bifunctional cross-linker sulfo-SMCC allowed for a simple conjugation protocol between the IgG proteins and the QDs. Bioconjugation and shell growth were both confirmed through the use of agarose gel electrophoresis. Bioactivity and binding specificity were investigated using streptavidin−maleimide and biotinylated microspheres and visualized under white and UV light. The slow growth of the as-synthesized water-soluble CdTe nanoparticles allows for multiple aliquots of increasing emission wavelength to be extracted during one synthesis. The silica shell provides a versatile platform for the decoration of the surface with specific functional groups to be later used for bioconjugation (thiols, carboxylic acids, amines), reduction of nonspecific binding (PEG), and increased biocompatibility.[25] In fact, studies of cell proliferation and apoptosis and necrosis have clearly indicated that silica-coated CdSe/ZnS QDs are the less detrimental species to live cells, a fact attributed to the reduced release of toxic Cd^{2+} ions into the organisms. Recent toxicological studies at the genetic level of cells transfected with silanized CdSe/ZnS indicate that the changes in gene expression are remarkably insignificant for more than 22 000 different gene spots.[26] In a peculiar result, silanized QDs do not elicit genes involved in the cellular response to heavy metal ion exposure. Thus, if we could further grow CdTe QDs into the near-IR spectrum, our ability to grow a silica shell would render these quantum dots highly soluble, brightly fluorescent, photostable, but most importantly neutral (nontoxic) to live organisms. Our proven ability to functionalize these silanized CdTe QDs with antibodies confers a biospecificity to these probes. As a consequence, silanized CdTe QDs properly functionalized hold great promise for noncytotoxic, site-directed surgeries, and in vivo bioimaging.

Acknowledgment. We are grateful to financial support from Petroleum Research Fund administered by the American Chemical Society, the National Science Foundation (NSF), and the University of California, Santa Cruz, Special Faculty Research Fund (J.Z.Z.). Part of this work was performed under the auspices of the U. S. Department of Energy by the University of California at the Lawrence Livermore National Laboratory under Contract No. W-7405-Eng-48. We thank Tevye Ryan Kuykendall for the HRTEM images and Joshua Deschamps for insightful recommendations. S.C. thanks the NSF for support (Grant No. CHE-0456130).

References and Notes

(1) Mattoussi, H.; Mauro, J. M.; Goldman, E. R.; Anderson, G. P.; Sundar, V. C.; Mikulec, F. V.; Bawendi, M. G. *J. Am. Chem. Soc.* **2000**, *122*, 12142−12150.

(2) Chan, W. C. W.; Nie, S. M. *Science* **1998**, *281*, 2016−2018.

(3) Parak, W. J.; Gerion, D.; Pellegrino, T.; Zanchet, D.; Micheel, C.; Williams, S. C.; Boudreau, R.; Le Gros, M. A.; Larabell, C. A.; Alivisatos, A. P. *Nanotechnology* **2003**, *14*, R15−R27.

(4) Bruchez, M.; Moronne, M.; Gin, P.; Weiss, S.; Alivisatos, A. P. *Science* **1998**, *281*, 2013−2016.

(5) Murray, C. B.; Norris, D. J.; Bawendi, M. G. *J. Am. Chem. Soc.* **1993**, *115*, 8706−8715.

(6) Gerion, D.; Pinaud, F.; Williams, S. C.; Parak, W. J.; Zanchet, D.; Weiss, S.; Alivisatos, A. P. *J. Phys. Chem. B* **2001**, *105*, 8861−8871.

(7) Gaponik, N.; Talapin, D. V.; Rogach, A. L.; Hoppe, K.; Shevchenko, E. V.; Kornowski, A.; Eychmuller, A.; Weller, H. *J. Phys. Chem. B* **2002**, *106*, 7177−7185.

(8) Dabbousi, B. O.; RodriguezViejo, J.; Mikulec, F. V.; Heine, J. R.; Mattoussi, H.; Ober, R.; Jensen, K. F.; Bawendi, M. G. *J. Phys. Chem. B* **1997**, *101*, 9463−9475.

(9) Goldman, E. R.; Balighian, E. D.; Kuno, M. K.; Labrenz, S.; Tran, P. T.; Anderson, G. P.; Mauro, J. M.; Mattoussi, H. *Phys. Status Solidi B* **2002**, *229*, 407−414.

(10) Kim, S.; Lim, Y. T.; Soltesz, E. G.; De Grand, A. M.; Lee, J.; Nakayama, A.; Parker, J. A.; Mihaljevic, T.; Laurence, R. G.; Dor, D. M.; Cohn, L. H.; Bawendi, M. G.; Frangioni, J. V. *Nat. Biotechnol.* **2004**, *22*, 93−97.

(11) Goldman, E. R.; Clapp, A. R.; Anderson, G. P.; Uyeda, H. T.; Mauro, J. M.; Medintz, I. L.; Mattoussi, H. *Anal. Chem.* **2004**, *76*, 684−688.

(12) Gerion, D.; Parak, W. J.; Williams, S. C.; Zanchet, D.; Micheel, C. M.; Alivisatos, A. P. *J. Am. Chem. Soc.* **2002**, *124*, 7070−7074.

(13) Mamedova, N. N.; Kotov, N. A.; Rogach, A. L.; Studer, J. *Nano Lett.* **2001**, *1*, 281−286.

(14) Wang, S. P.; Mamedova, N.; Kotov, N. A.; Chen, W.; Studer, J. *Nano Lett.* **2002**, *2*, 817−822.

(15) Pathak, S.; Choi, S. K.; Arnheim, N.; Thompson, M. E. *J. Am. Chem. Soc.* **2001**, *123*, 4103−4104.

(16) Derfus, A. M.; Chan, W. C. W.; Bhatia, S. N. *Nano Lett.* **2004**, *4*, 11−18.

(17) Liz-Marzan, L. M.; Giersig, M.; Mulvaney, P. *Langmuir* **1996**, *12*, 4329−4335.

(18) Doering, W. E.; Nie, S. M. *Anal. Chem.* **2003**, *75*, 6171−6176.

(19) Kobayashi, Y.; Misawa, K.; Takeda, M.; Kobayashi, M.; Satake, M.; Kawazoe, Y.; Ohuchi, N.; Kasuya, A.; Konno, M. *Colloids Surf., A* **2004**, *251*, 197−201.

(20) Rogach, A. L.; Nagesha, D.; Ostrander, J. W.; Giersig, M.; Kotov, N. A. *Chem. Mater.* **2000**, *12*, 2676−2685.

(21) Ung, T.; Liz-Marzan, L. M.; Mulvaney, P. *J. Phys. Chem. B* **1999**, *103*, 6770−6773.

(22) Wang, Y.; Tang, Z. Y.; Liang, X. R.; Liz-Marzan, L. M.; Kotov, N. A. *Nano Lett.* **2004**, *4*, 225−231.

(23) Correa-Duarte, M. A.; Giersig, M.; Liz-Marzan, L. M. *Chem. Phys. Lett.* **1998**, *286*, 497−501.

(24) Schroedter, A.; Weller, H.; Eritja, R.; Ford, W. E.; Wessels, J. M. *Nano Lett.* **2002**, *2*, 1363−1367.

(25) Kirchner, C.; Liedl, T.; Kudera, S.; Pellegrino, T.; Javier, A. M.; Gaub, H. E.; Stolzle, S.; Fertig, N.; Parak, W. J. *Nano Lett.* **2005**, *5*, 331−338.

(26) Zhang, T.; Gerion, D.; Elboudwarej, O.; Cooke, P. A.; Alivisatos, A. P.; Gray, J. W.; CHen, F. F., to be submitted for publication.

(27) Stone, K. R.; Mickey, D. D.; Wunderli, H.; Mickey, G. H.; Paulson, D. F. *Int. J. Cancer* **1978**, *21*, 274−281.

(28) Peng, X. G.; Wickham, J.; Alivisatos, A. P. *J. Am. Chem. Soc.* **1998**, *120*, 5343−5344.

(29) Talapin, D. V.; Rogach, A. L.; Shevchenko, E. V.; Kornowski, A.; Haase, M.; Weller, H. *J. Am. Chem. Soc.* **2002**, *124*, 5782−5790.

(30) Karstens, T.; Kobs, K. *J. Phys. Chem.* **1980**, *84*, 1871−1872.

(31) Doose, S.; Tsay, J. M.; Pinaud, F.; Weiss, S. *Anal. Chem.* **2005**, *77*, 2235−2242.

(32) Yu, W. W.; Qu, L. H.; Guo, W. Z.; Peng, X. G. *Chem. Mater.* **2003**, *15*, 2854−2860.

(33) Hintermann, G.; Fischer, H. M.; Crameri, R.; Hutter, R. *Plasmid* **1981**, *5*, 371−373.

(34) Slater, G. W.; Noolandi, J. *Biopolymers* **1989**, *28*, 1781−1791.

(35) Ströber, W. F., A.; Bohn, E. J. *J. Colloid Interface Sci.* **1968**, *26*.

(36) Chemseddine, A.; Weller, H. *Ber. Bunsen−Ges. Phys. Chem.* **1993**, *97*, 636−637.

(37) Yoshitake, S.; Yamada, Y.; Ishikawa, E.; Masseyeff, R. *Eur. J. Biochem.* **1979**, *18*, 395−399.

(38) Kitagawa, T.; Aikawa, T. *J. Biochem.* **1976**, *15*, 233−236.

(39) Kim, I. S.; Lee, S. K.; Park, Y. M.; Lee, Y. B.; Shin, S. C.; Lee, K. C.; Oh, I. J. *Int. J. Pharm.* **2005**, *298*, 255−262.

(40) Gould, E. A.; Buckley, A.; Cammack, N. *J. Virol. Methods* **1985**, *11*, 41−48.

(41) Zhang, F.; Kang, E. T.; Neoh, K. G.; Wang, P.; Tan, K. L. *Biomaterials* **2001**, *22*, 1541−1548.

(42) Parak, W. J.; Gerion, D.; Zanchet, D.; Woerz, A. S.; Pellegrino, T.; Micheel, C.; Williams, S. C.; Seitz, M.; Bruehl, R. E.; Bryant, Z.; Bustamante, C.; Bertozzi, C. R.; Alivisatos, A. P. *Chem. Mater.* **2002**, *14*, 2113−2119.